Frontiers of Information Technology & Electronic Engineering
www.jzus.zju.edu.cn; engineering.cae.cn; www.springerlink.com
ISSN 2095-9184 (print); ISSN 2095-9230 (online)
E-mail: jzus@zju.edu.cn

Pulse control of frequency and width for a real-time independently adjustable laser source*

Zhiwei YANG[1,2], Xu WU[†‡1,2], Deqin OUYANG[2], Encheng ZHANG[2], Huibin SUN[1], Shuangchen RUAN[†‡1,2]

[1]*Guangdong Provincial Key Laboratory of Micro/Nano Optomechatronics Engineering, College of Physics Science and Optoelectronic Engineering, Shenzhen University, Shenzhen 518060, China*

[2]*College of Sino-German Intelligent Manufacturing, Shenzhen Technology University, Shenzhen 518118, China*

[†]E-mail: wuxu@sztu.edu.cn; scruan@szu.edu.cn

Received June 18, 2020; Revision accepted Nov. 8, 2020; Crosschecked Feb. 1, 2021; Published online Mar. 29, 2021

Abstract: A set of semiconductor laser pulse seed sources based on an embedded chip is proposed. The greatest feature is that the optical pulse frequency and width can be independently adjusted in real time. The pulse seed sources can be switched independently and online from the gain-switched mode to the quasi-continuous wave mode to obtain optimal optical parameters for specific applications. To explore the physical mechanism of the semiconductor laser source, the rate equation that describes the carrier-photon transient change in a semiconductor laser cavity is numerically derived and solved. Subsequently, problems that need to be considered while designing the drive circuit are identified. The system evaluation indicates that the optical pulse frequency adjustment range is 250 Hz to 42 MHz, and the narrowest optical pulse output width is 80 ps. The pulse seed source can drive semiconductor lasers with different central wavelengths (1064, 1550, and 1970 nm), and can also simultaneously drive two semiconductor lasers and output dual-band optical pulses. It can be used as a seed source for general high-power optical systems, and exhibits good application value and extensive market prospects.

Key words: Electric variable control; Electronic design automation and methodology; Optical pulse generation; Optical control
https://doi.org/10.1631/FITEE.2000294 **CLC number:** TN78

1 Introduction

Picosecond laser pulses have important applications in various fields, such as quantum communication (Abellán et al., 2014; Nakata et al., 2017; Xie et al., 2019), optical measurement (Pascual et al., 2015; Wada et al., 2015; Lakshmijayasimha et al., 2019), and nonlinear optics (Hatami et al., 2006; Fang et al., 2016; Hu et al., 2019). Mode-locked, Q-switched, and gain-switched technologies are commonly used in short-pulse laser generation methods, and can be used to generate pulsed laser outputs exhibiting different repetition frequencies, pulse widths, and powers. The gain-switched semiconductor laser has a simpler structure, more flexible setting, more stable performance, and continuous adjustment of repetitive frequency, compared with Q-switched and mode-locking technologies. The combination of the gain-switched semiconductor laser as a seed source and the high-power fiber amplification technology has significantly improved the laser performance. This combination has been extensively used in various fields, and it demonstrates significant development potential. Quasi-continuous

‡ Corresponding authors

* Project supported by the Basic Research Foundation of Knowledge Innovation Program of Shenzhen City, China (No. JCYJ20180301-171044707) and the University-Enterprise Cooperation Research and Development Project of Shenzhen Technology University, China (Nos. 2018010802002, 2018010802005, and 2019310103001)

ORCID: Zhiwei YANG, https://orcid.org/0000-0003-0715-9877; Xu WU, https://orcid.org/0000-0002-1176-8440; Shuangchen RUAN, https://orcid.org/0000-0001-7478-8054

wave (QCW) lasers operate in both continuous and high-peak-power pulse modes. Therefore, high-energy microsecond and millisecond pulses can be generated at repetitive frequencies ranging from tens to thousands of hertz, and the suitable average and peak powers can be achieved at the kilowatt level (Kulygin et al., 2017; Xiao et al., 2017; Hong et al., 2018; Li et al., 2019). A QCW fiber laser containing a QCW semiconductor laser as a seed source combined with the high-power fiber amplification technology is extensively used in the welding and marking of precision devices and medical equipment because of its high average power and adjustable pulse repetition frequency. Furthermore, processing speed and production efficiency are significantly improved.

The gain-switched semiconductor laser technology exhibiting various pulse widths has been developed. Dupriez et al. (2006) constructed a Yb-doped optical fiber master oscillator power amplifier (MOPA) structure using a gain-switched semiconductor seed source with a pulse width of 56 ps. After multistage amplification, the average power was 321 W, the pulse width was 20 ps, and the pulse repetition rate was 1 GHz. Liu et al. (2008) used a commercial gain-switched semiconductor laser with a pulse width of 70 ps and a repetition frequency of 1 MHz as the seed source. The average power with a repetition frequency of 1 MHz was 3.5 W, and a pulse width of 90 ps was obtained using an amplification system. Kanzelmeyer et al. (2011) amplified a commercial gain-switched semiconductor laser with a repetition frequency of 1 MHz and a pulse width of 37 ps using all-fiber devices to obtain a pulse width of 40 ps and a peak power of 270 kW. Heidt et al. (2013) first injected a thulium-doped fiber amplifier with a 2-μm gain-switched semiconductor seed. A gain-switched optical pulse with a pulse width of 33 ps was obtained. The average power was 18 W after amplification. Lin et al. (2018) constructed a Yb-doped optical fiber MOPA structure using a gain-switched semiconductor seed source with a central wavelength of 1030 nm and a pulse width of 150 ps. An output beam with an average power of 106 W and a pulse width of 110 ps was obtained.

For a sinusoidal signal, frequency is directly related to the pulse width; i.e., the higher the frequency, the narrower the pulse width. In the case of a sinusoidal wave, the changes in the frequency and pulse width are observed simultaneously. In particular, sinusoidal modulation is undesirable in applications that require a low frequency and a narrow pulse width. Furthermore, a novel embedded technology has been proposed and applied to high-power optical fiber lasers to resolve the above problem. For example, semiconductor lasers are modulated using analog control and internal pulse generators, and a set of multi-functional seed sources with independent and real-time adjustable pulse frequency and width has been proposed. We can switch online the pulse seed source from the gain-switched mode to the QCW mode to obtain optimal optical parameters for specific applications. The rate equation that describes the carrier-photon transient change in a semiconductor laser cavity is numerically derived and solved. Subsequently, the effects of electrical signal and semiconductor laser parameters on the output pulse waveform are simulated and analyzed. Furthermore, the hardware design of the optical pulse seed source is described, and details of the design process are analyzed.

2 Experimental setup

2.1 Modulation characteristics of semiconductor lasers

Rate equations can be employed to analyze the relationship between the dynamic characteristics of semiconductor lasers and various device parameters. Rate equations can also be used to establish the relationship between photons and carriers (Murakami et al., 2003; Wieczorek et al., 2005; Klein et al., 2006; Holub et al., 2007; Jirauschek and Kubis, 2014). The carrier density is correlated with the pump current density using the rate equation, which considers all the carrier generation mechanisms and loss in the active region. The general form of the carrier rate equation can be given as follows:

$$\frac{\partial N}{\partial t} = D(\nabla^2 N) + \frac{I}{ed} - R(N), \tag{1}$$

where N denotes the number of inverted particles, I the pumping current, e the electronic charge, and d the length of the active region.

At the right side of Eq. (1), the first term is the

carrier diffusion, the second term the carrier injection rate into the active region, and the final term the carrier loss obtained using various recombination processes. Regardless of the carrier diffusion, Eq. (1) can be simplified as

$$\frac{\partial N}{\partial t}=\frac{I}{e}-\gamma_e N-G\cdot P, \tag{2}$$

where γ_e denotes the carrier recombination rate, G the net stimulated emission rate, P the number of photons, and $G\cdot P$ the stimulated recombination results obtained based on the nonlinear coupling between photons and carriers. According to the deduced photon motion amplitude and phase rate equation, the photon number amplitude can be expressed as

$$\frac{\partial P}{\partial t}=(G-\gamma)P+R_{\mathrm{sp}}, \tag{3}$$

where γ is the photon decay rate, and R_{sp} is the photon number change rate at which spontaneous emission photons are transformed into stimulated emission photons. $R_{\mathrm{sp}}=\beta\gamma_e N$, where β is the portion of the spontaneously emitted photons converted into the stimulated radiation modes.

MATLAB is used to numerically solve the rate equation of a semiconductor laser, to investigate the influence of the change of external electrical signal parameters on the output characteristics of the gain-switched semiconductor laser. The simulation results can guide the selection of the electrical signal parameters to produce optical pulses exhibiting high-quality parameters.

Fig. 1a shows the effects of the modulation frequency on the output optical pulse waveform. With an increase in the modulation frequency, the current is cut off before reaching saturation; therefore, the amplitude of the optical pulse decreases. A tailing phenomenon can be observed at the back end of the optical pulse when the modulation frequency is low. The lower the modulation frequency, the more obvious the tailing phenomenon. Figs. 1b and 1c denote the effects of the output frequency on the optical pulse parameters. The pulse width of the optical pulse initially increases and subsequently decreases with an increase in the modulation frequency. The change trend of the rise time of the optical pulse is similar to that of the optical pulse.

Fig. 2a denotes the effects of the magnitude of the signal amplitude on the output optical pulse waveform, whereas Figs. 2b and 2c show the optical pulse parameters as a function of the signal magnitude. With an increase in the amplitude of the electrical signal, the optical pulse amplitude increases, the pulse width decreases, and the rise time of the optical pulse decreases. However, the optical pulse trailing phenomenon can be observed after an increase in the amplitude of the electrical signal. The pulse phenomenon can be optimized by changing the remaining electrical signal parameters. It can be observed in Fig. 3a that decreasing the offset can eliminate the pulse tailing phenomenon. With an increase in the amplitude of the electrical signal, the carrier time for the first generation of the optical pulse decreases; the rise time of the carrier also decreases, and the decreasing trend is greater.

Fig. 3a denotes the effects of the magnitude of the electrical signal offset on the output optical pulse waveform. The optical pulse parameters as a function of the electrical signal bias are plotted in Figs. 3b and 3c. The tailing phenomenon of the optical pulse becomes more obvious as the direct current (DC) offset increases. The trailing pulse occupies part of the pulse energy; thus, the amplitude of the output optical pulse tends to decrease. The pulse width initially decreases and subsequently increases. Therefore, the bias current should not be high in practical applications. Generally, the bias current is set near or lower than the threshold current.

2.2 Semiconductor laser seed source design principle

The core components of the driving circuit for a semiconductor pulsed seed source include an initial pulse generator, a pulse compression and shaping module, a pulse adjustable amplification module, a constant-current source (CCS) module, a temperature control module, a power supply module, and some peripheral circuits. The driving circuit is presented in Fig. 4. The initial pulse is generated using an STM32F407ZGT6 (STM32F4) microcontroller based on the pulse width modulation (PWM) principle, which is a digital coding method for analog signals. Using a high-resolution counter, the duty cycle of a square wave is invoked to encode the level of a specific analog signal. When the output frequency of the

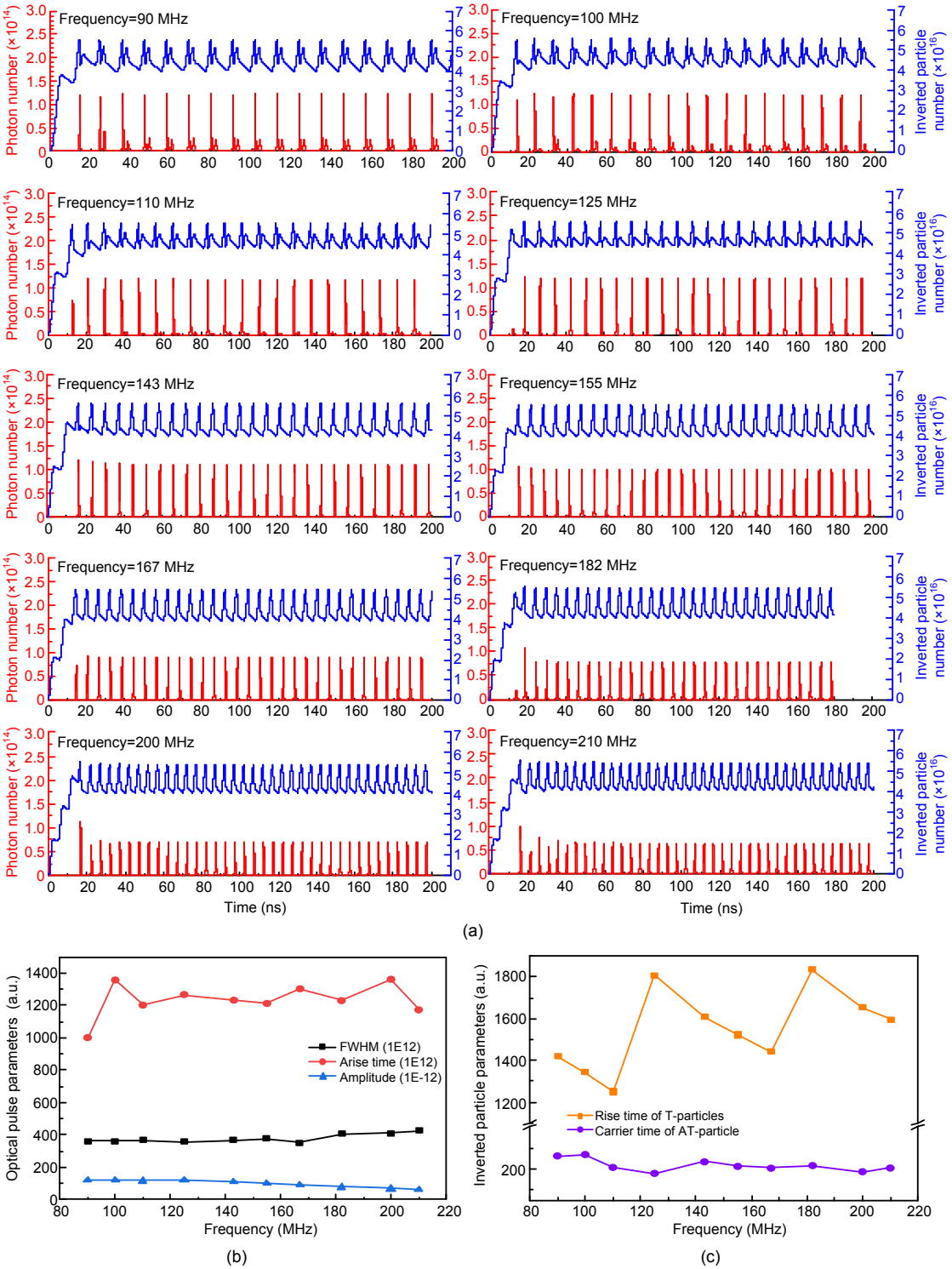

Fig. 1 Effects of the modulation frequency on the output optical pulse waveform (a), optical pulse waveform parameters (b), and inverted particle parameters (c)

In (a), the red curves denote the photon number, and blue curves denote the inverted particle number. In (b), the red line indicates the rise time of the optical pulse, the black line indicates the full width at half maximum (FWHM) of the optical pulse, and the blue line indicates the amplitude of the optical pulse. In (c), the orange line indicates the rise time of the carriers (T-particles), and the purple line indicates the carrier time at which the pulse was initially generated (AT-particle). References to color refer to the online version of this figure

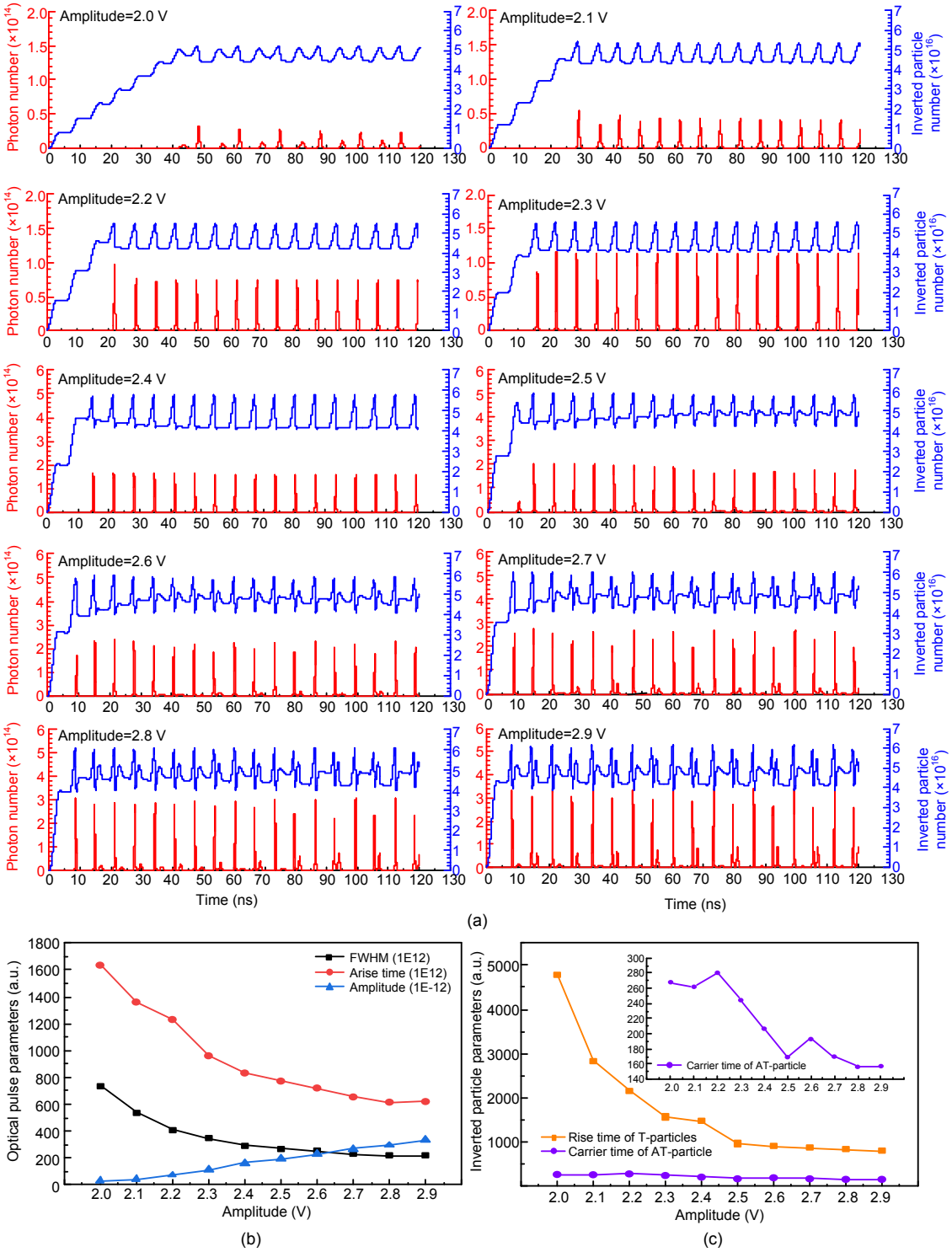

Fig. 2 Effects of the magnitude of the signal amplitude on the output optical pulse waveform (a), optical pulse waveform parameters (b), and inverted particle parameters (c)

In (a), the red curves denote the photon number, and blue curves denote the inverted particle number. In (b), the red line indicates the rise time of the optical pulse, the black line indicates the full width at half maximum (FWHM) of the optical pulse, and the blue line indicates the amplitude of the optical pulse. In (c), the orange line indicates the rise time of the carriers (T-particles), and the purple line indicates the carrier time at which the pulse was initially generated (AT-particle). References to color refer to the online version of this figure

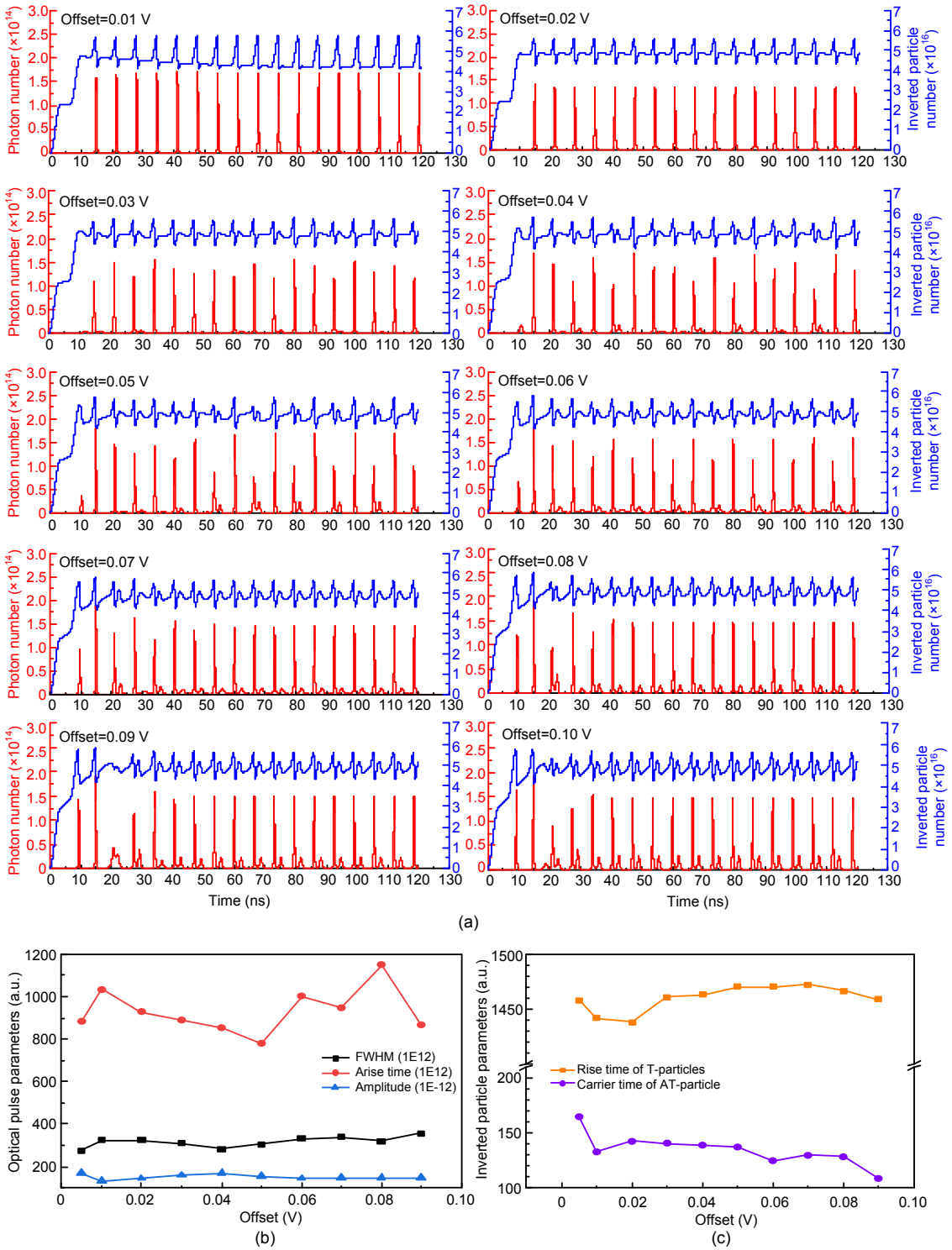

Fig. 3 Effects of the magnitude of the electrical signal offset on the output optical pulse waveform (a), optical pulse waveform parameters (b), and inverted particle parameters (c)

In (a), the red curves denote the photon number, and blue curves denote the inverted particle number. In (b), the red line indicates the rise time of the optical pulse, the black line indicates the full width at half maximum (FWHM) of the optical pulse, and the blue line indicates the amplitude of the optical pulse. In (c), the orange line indicates the rise time of the carriers (T-particles), and the purple line indicates the carrier time at which the pulse was initially generated (AT-particle). References to color refer to the online version of this figure

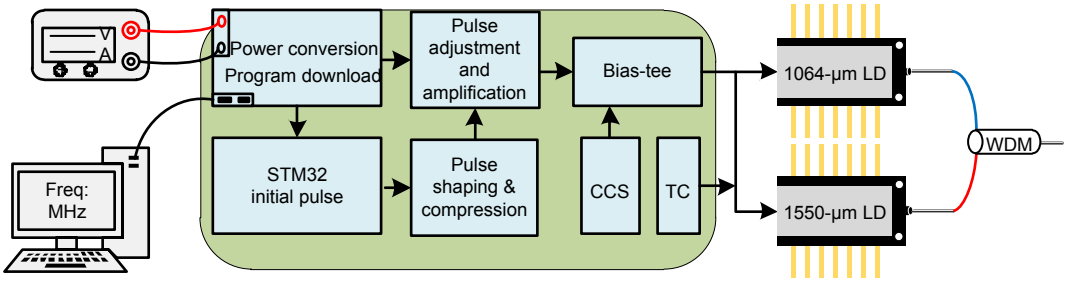

Fig. 4 A block diagram of the driving circuit

CCS: constant-current source; TC: temperature control; LD: laser diode; WDM: wavelength division multiplexing

control circuit is unchanged, the duty cycle is adjusted based on the voltage feedback to obtain a stable adjustable pulse width output (Singh et al., 1999; Blaabjerg et al., 2006). The main frequency of STM32F4 is 168 MHz. According to the Nyquist sampling theorem, in practice, the sampling frequency should be 2.56 to 4 times the maximum frequency of the signal; thus, the maximum pulse generation frequency is 42 MHz. The pulse width of the initial electrical signal is narrowed using a digital signal pulse width compressor, and the pulse of the electrical signal is shaped to eliminate the trailing. Subsequently, the shaping pulse is amplified using a high-speed, low-distortion current feedback operational amplifier. The high-precision resistance can accurately modulate the amplification factor such that the pulse power is suitable for various parameters. The CCS module outputs a highly stable current based on the current series negative feedback principle and biases the laser diode (LD) to ensure its stable operation. The coupling circuit superimposes the pulse AC signal and the constant-current DC signal onto the LD. The temperature control module employs a temperature control chip to acquire the internal temperature of the LD and control the thermoelectric cooler to ensure the stable operation of the LD. In addition, the temperature control module protects the LD.

We avoid reflection, crosstalk, and other problems that may occur during the signal transmission process to reduce the loss of the pulse signal. We have performed calculations and developed layouts for the wring and design of the circuit (Ionescu and Riel, 2011; Lu et al., 2013; Yu and Kang, 2020; Zang et al., 2020). Our design of the semiconductor laser seed source is presented in Fig. 5. Furthermore, we can ensure the integrity of the signal transmission to

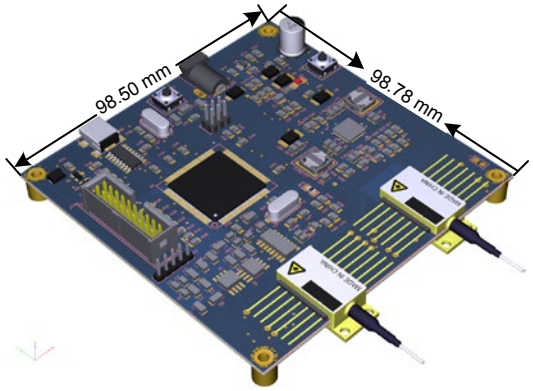

Fig. 5 Design of the semiconductor laser seed source

reduce pulse signal loss and simultaneously avoid the reflection, crosstalk, and other problems that may occur during the signal transmission. To reduce the amount of crosstalk as much as possible, we add a protective ground line to the periphery of the signal traces, and the signal line to be protected is added in the middle. Simultaneously, one or several high-frequency decoupling capacitors are placed in the vicinity of each integrated circuit block. A nearby high-frequency channel is obtained for the transient current of the integrated circuit. Consequently, the transient current does not pass through the power supply line with a large loop area, considerably reducing the outward radiated noise. Each integrated chip has its high-frequency channel. There is no common impedance between them, thus suppressing the impedance coupling.

3 Results and analysis

The semiconductor lasers used in the experiments were 1064-nm Fabry-Perot (FP) (LC96A1064NBFBG-20R), 1550-nm distributed

feedback (DFB) (SWLD-155120S22-01), and 1970-nm discrete mode (DM) (EP1970-0-DM-B06-FM). The laser output was measured using a spectrometer to obtain the frequency-domain characteristics, and the time-domain characteristics were detected using high-speed photodetectors (New Focus, Model-1024-45G and EOT ET-5000) and oscilloscopes (Teledyne LeCroy, SDA 820Zi-B 20G). The semiconductor laser was soldered to the designed driver board. The output pulse spectra are presented in Fig. 6. Figs. 6a, 6b, and 6c are the output pulse spectra for the 1064, 1550, and 1970 nm lasers, respectively. The 3-dB spectral widths are 3.026, 0.052, and 0.1486 nm, respectively. Fig. 6d shows the dual-wavelength pulse spectrum of two lasers simultaneously soldered to the driver board. The fixed signal frequency is 1 MHz, the pulse duty ratio is set to the minimum, and the signal output amplitude is adjusted to cause the semiconductor laser to generate the gain switching effects. The optical power corresponding to the threshold current is small based on the *P-I* curve of the semiconductor laser. STM32F4 generated an electrical pulse with an initial pulse width of 6 ns; the 6-ns electrical pulse was compressed to the shortest by adjusting the compression factor of the pulse compressor. The narrowest electrical pulse width is 1 ns. The amplification factor of the amplifier was adjusted, and the amplified electric pulse drove the semiconductor laser to enable the production of a narrow optical pulse. As shown in Fig. 7a, the output waveform exhibits an FWHM of 80 ps without tailing. The frequency of the driving signal is 1 MHz. The electrical pulse duty ratio was set to the maximum. STM32F4 generated an electrical pulse with an initial pulse width of 980 ns. The amplification factor of the amplifier was adjusted, and the amplified electric pulse drove the semiconductor laser to enable it to produce a 980-ns optical pulse. As shown in Fig. 7b, the optical pulse output with a pulse width of 980 ns is stable, and the base is small.

As shown in Fig. 8a, the drive signal frequency is set to a minimum of 250 Hz, the duty ratio is set to 50%, and the amplitude of the adjustment signal is obtained as an optical pulse output with a frequency of 250 Hz. Setting the drive signal frequency to a maximum of 42 MHz and adjusting the amplitude of the signal can obtain an optical pulse output with a frequency of 42 MHz, as shown in Fig. 8b. Fig. 9a

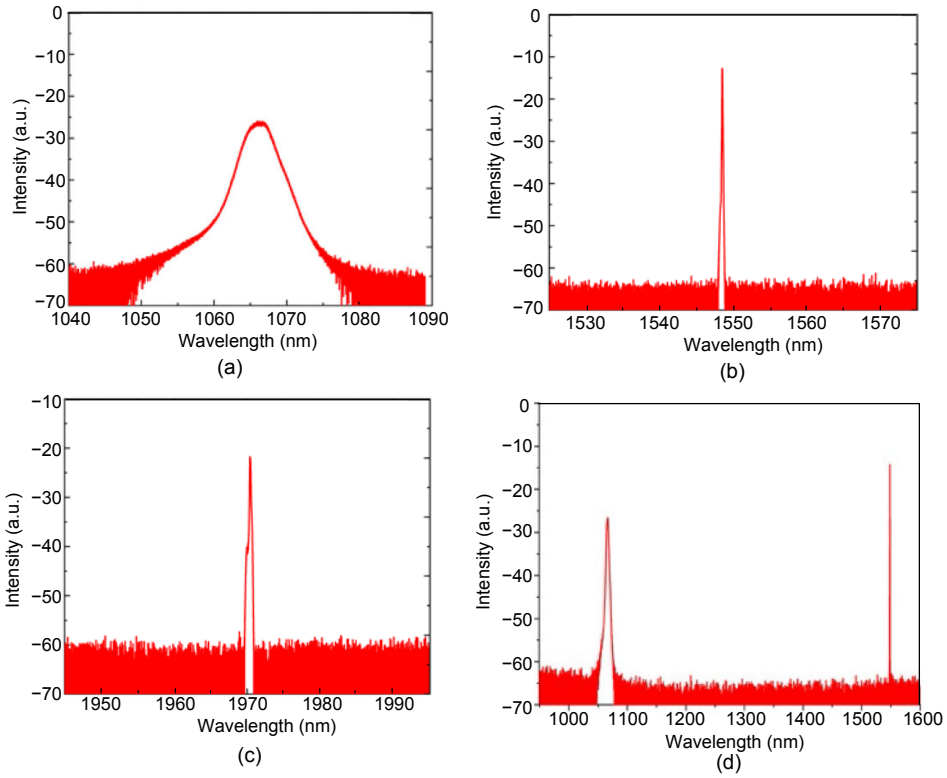

Fig. 6 Output pulse spectra with 1064 (a), 1550 (b), and 1970 (c) nm lasers and dual-wavelength pulse spectrum of two lasers with dual wavelength=1064 nm/1550 nm (d)

shows the optical pulses with a frequency of 1 MHz and widths of 0.1, 1, 10, and 100 ns. In Fig. 9b, the FWHM is 1 ns and the frequencies are 0.1, 1, 5, and 10 MHz. The peak power of the pulse is basically maintained at 0.8 mW. The frequency of the output optical pulse ranges from 250 Hz to 42 MHz, and the minimum pulse width of the optical pulse is 80 ps. The gain switching optical pulse and the quasi-to-continuous pulse output are simultaneously satisfied.

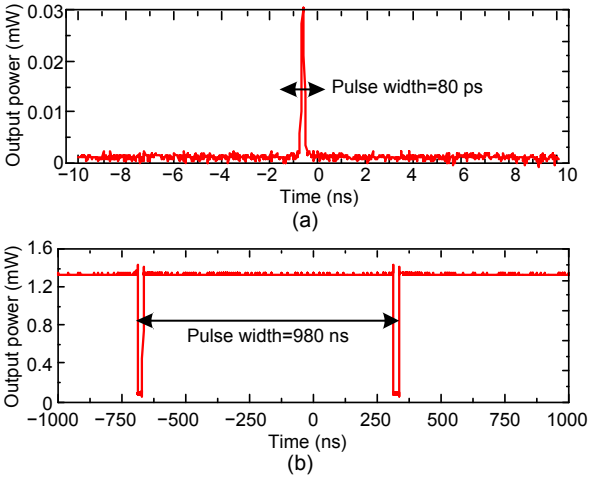

Fig. 7 Optical pulse output with spectral widths of 80 ps (a) and 980 ns (b)

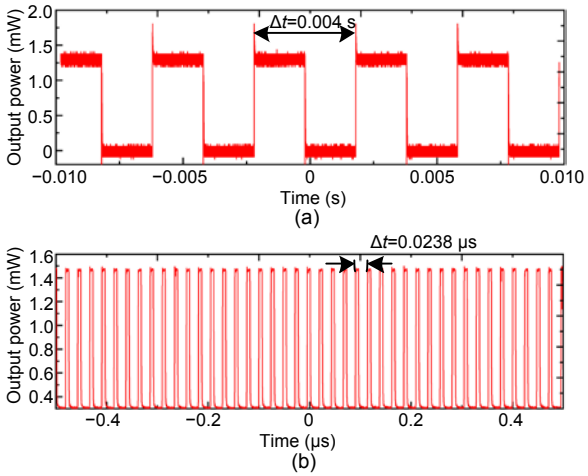

Fig. 8 Optical pulse output with frequencies of 250 Hz (a) and 42 MHz (b)

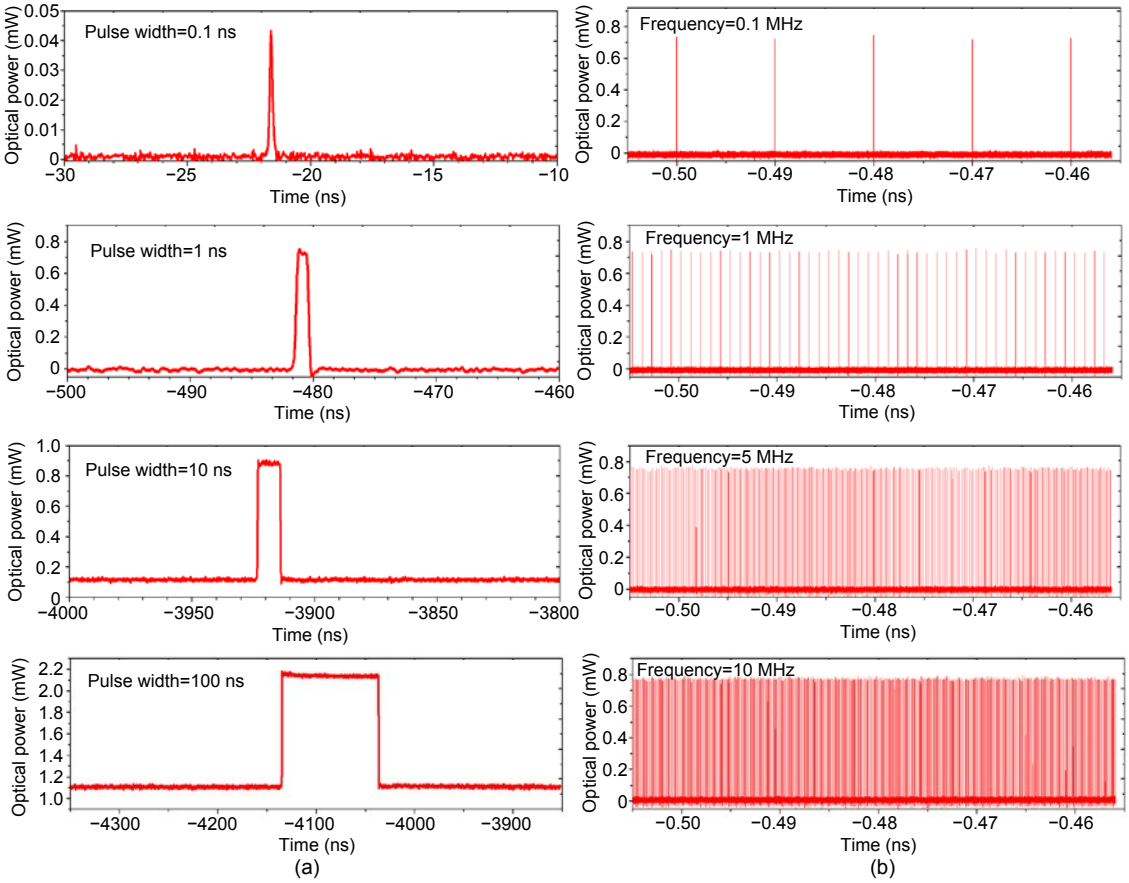

Fig. 9 Optical pulses with a frequency of 1 MHz and pulse widths of 0.1, 1, 10, and 100 ns (a) and optical pulses with full width at half maximum of 1 ns and frequencies of 0.1, 1, 5, and 10 MHz (b)

4 Conclusions

A set of fiber laser pulse sources with adjustable optical signal parameters has been obtained using an embedded technology design. Furthermore, a rate equation model has been established and analyzed for a semiconductor laser; the accuracy of the model has been experimentally verified. When compared with the driving of traditional semiconductor lasers, the frequency and pulse width of the laser pulse source in this study can be separately modulated, considerably increasing the application range of the seed source. The designed drive circuit exhibits a compact structure, adjustable pulse width and frequency, and high stability. The experimental results demonstrated that the laser pulse optical source exhibits stable output power and a high signal-to-noise ratio. It can be used as a seed source for general high-power optical systems, and exhibits good application value and extensive market prospects.

Contributors

Xu WU and Shuangchen RUAN proposed the idea. Zhiwei YANG, Xu WU, and Shuangchen RUAN designed the research. Zhiwei YANG processed the data and drafted the manuscript. Deqin OUYANG, Encheng ZHANG, and Huibin SUN helped organize the manuscript. Xu Wu and Shuangchen RUAN revised and finalized the paper.

Compliance with ethics guidelines

Zhiwei YANG, Xu WU, Deqin OUYANG, Encheng ZHANG, Huibin SUN, and Shuangchen RUAN declare that they have no conflict of interest.

References

Abellán C, Amaya W, Jofre M, et al., 2014. Ultra-fast quantum randomness generation by accelerated phase diffusion in a pulsed laser diode. *Opt Expr*, 22(2):1645-1654. https://doi.org/10.1364/oe.22.001645

Blaabjerg F, Teodorescu R, Liserre M, et al., 2006. Overview of control and grid synchronization for distributed power generation systems. *IEEE Trans Ind Electron*, 53(5): 1398-1409. https://doi.org/10.1109/TIE.2006.881997

Dupriez P, Piper A, Malinowski A, et al., 2006. High average power, high repetition rate, picosecond pulsed fiber master oscillator power amplifier source seeded by a gain-switched laser diode at 1060 nm. *IEEE Photon Technol Lett*, 18(9):1013-1015. https://doi.org/10.1109/LPT.2006.873486

Fang YC, Chaki T, Hung JH, et al., 2016. 1 MW peak-power subpicosecond optical pulse source based on a gain-switched laser diode. *Opt Lett*, 41(17):4028-4031. https://doi.org/10.1364/ol.41.004028

Hatami M, Ghafouri-Shiraz H, Zakery A, 2006. Analysis of a gained nonlinear directional coupler pulse switch. *Opt Quant Electron*, 38(15):1259-1268. https://doi.org/10.1007/s11082-007-9059-7

Heidt AM, Li Z, Sahu J, et al., 2013. 35 kW peak power picosecond pulsed thulium-doped fibre amplifier system seeded by a gain-switched laser diode at 2 μm. Conf on Lasers & Electro-Optics Europe & Int Quantum Electronics Conf, p.1615-1617. https://doi.org/10.1109/CLEOE-IQEC.2013.6801304

Holub M, Shin J, Saha D, et al., 2007. Electrical spin injection and threshold reduction in a semiconductor laser. *Phys Rev Lett*, 98(14):146603. https://doi.org/10.1103/PhysRevLett.98.146603

Hong S, Kong B, Lee YS, et al., 2018. Pulse control in a wide frequency range for a quasi-continuous wave diode-pumped cesium atom vapor laser by a pump modulation in the spectral domain. *Opt Expr*, 26(20):26679-26687. https://doi.org/10.1364/oe.26.026679

Hu PC, Chang D, Tan JB, et al., 2019. Displacement measuring grating interferometer: a review. *Front Inform Technol Electron Eng*, 20(5):631-654. https://doi.org/10.1631/FITEE.1800708

Ionescu AM, Riel H, 2011. Tunnel field-effect transistors as energy-efficient electronic switches. *Nature*, 479(7373): 329-337. https://doi.org/10.1038/nature10679

Jirauschek C, Kubis T, 2014. Modeling techniques for quantum cascade lasers. *Appl Phys Rev*, 1(1):011307. https://doi.org/10.1063/1.4863665

Kanzelmeyer S, Sayinc H, Theeg T, et al., 2011. All-fiber based amplification of 40 ps pulses from a gain-switched laser diode. *Opt Expr*, 19(3):1854-1859. https://doi.org/10.1364/oe.19.001854

Klein E, Gross N, Rosenbluh M, et al., 2006. Stable isochronal synchronization of mutually coupled chaotic lasers. *Phys Rev E*, 73(6):066214. https://doi.org/10.1103/PhysRevE.73.066214

Kulygin M, Denisov G, Shubin S, et al., 2017. Subterahertz nanosecond switches driven by second-long laser pulses. *IEEE Trans Terahertz Sci Technol*, 7(2):225-227. https://doi.org/10.1109/TTHZ.2017.2647879

Lakshmijayasimha PD, Kaszubowska-Anandarajah A, Martin EP, et al., 2019. Expansion and phase correlation of gain-switched optical frequency combs through FWM in an SOA. Optical Fiber Communication Conf, p.16560-16570. https://doi.org/10.1364/OFC.2019.W1B.2

Li QF, Grojo D, Alloncle AP, et al., 2019. Jetting regimes of double-pulse laser-induced forward transfer. *Opt Mater Expr*, 9(8):3476-3486. https://doi.org/10.1364/ome.9.003476

Lin D, Baktash N, Alam SU, et al., 2018. 106 W, picosecond Yb-doped fiber MOPA system with a radially polarized output beam. *Opt Lett*, 43(20):4957-4960. https://doi.org/10.1364/ol.43.004957

Liu HJ, Gao CX, Tao JT, et al., 2008. Compact tunable high

power picosecond source based on Yb-doped fiber amplification of gain switch laser diode. *Opt Expr*, 64(11): 7888-7839. https://doi.org/10.1364/OE.16.007888

Lu LG, Han XB, Li JQ, et al., 2013. A review on the key issues for lithium-ion battery management in electric vehicles. *J Power Sources*, 226:272-288. https://doi.org/10.1016/j.jpowsour.2012.10.060

Murakami A, Kawashima K, Atsuki K, 2003. Corrections to "Cavity resonance shift and bandwidth enhancement in semiconductor lasers with strong light injection". *IEEE J Quant Electron*, 39(11):1504. https://doi.org/10.1109/JQE.2003.820130

Nakata K, Tomita A, Fujiwara M, et al., 2017. Intensity fluctuation of a gain-switched semiconductor laser for quantum key distribution systems. *Opt Expr*, 25(2):622-634. https://doi.org/10.1364/oe.25.000622

Pascual MDG, Zhou R, Smyth F, et al., 2015. Software reconfigurable highly flexible gain switched optical frequency comb source. *Opt Expr*, 23(18):23225-23235. https://doi.org/10.1364/oe.23.023225

Singh B, Al-haddad K, Chandra A, 1999. A review of active filters for power quality improvement. *IEEE Trans Ind Electron*, 46(5):960-971. https://doi.org/10.1109/41.793345

Wada K, Matsukura S, Tanaka A, et al., 2015. Precise measurement of single-mode fiber lengths using a gain-switched distributed feedback laser with delayed optical feedback. *Opt Expr*, 23(18):23013-23020. https://doi.org/10.1364/oe.23.023013

Wieczorek S, Krauskopf B, Simpson TB, et al., 2005. The dynamical complexity of optically injected semiconductor lasers. *Phys Rep*, 416(1-2):1-128. https://doi.org/10.1016/j.physrep.2005.06.003

Xiao H, Li SM, Han X, et al., 2017. Laves phase control of Inconel 718 alloy using quasi-continuous-wave laser additive manufacturing. *Mater Des*, 122:330-339. https://doi.org/10.1016/j.matdes.2017.03.004

Xie HB, Li Y, Jiang C, et al., 2019. Optically injected intensity-stable pulse source for secure quantum key distribution. *Opt Expr*, 27(9):12231-12240. https://doi.org/10.1364/oe.27.012231

Yu YM, Kang K, 2020. Analysis and design of transformer-based CMOS ultra-wideband millimeter-wave circuits for wireless applications: a review. *Front Inform Technol Electron Eng*, 21(1):97-115. https://doi.org/10.1631/FITEE.1900491

Zang YJ, Chen YH, Yang CJ, et al., 2020. A new approach for analyzing the effect of non-ideal power supply on a constant current underwater cabled system. *Front Inform Technol Electron Eng*, 21(4):604-614. https://doi.org/10.1631/FITEE.1800737